International Journal of Multiphase Flow 138 (2021) 103590

Contents lists available at ScienceDirect

International Journal of Multiphase Flow

journal homepage: www.elsevier.com/locate/ijmulflow

Upward and downward two-phase flow of CO_2 in a pipe: Comparison between experimental data and model predictions

Morten Hammer[a], Han Deng[a], Lan Liu[b], Morten Langsholt[b], Svend Tollak Munkejord[a,*]

[a] SINTEF Energy Research, P.O. Box 4761 Torgarden, Trondheim NO-7465, Norway
[b] Institute for Energy Technology, P.O. Box 40, Kjeller NO-2027, Norway

ARTICLE INFO

Article history:
Received 12 October 2020
Revised 28 January 2021
Accepted 8 February 2021
Available online 11 February 2021

Keywords:
Carbon dioxide
CO_2 injection
Vertical flow
Friction
Liquid holdup
Fluid dynamics
Thermodynamics

ABSTRACT

In order to deploy CO_2 capture and storage (CCS) systems to mitigate climate change, it is crucial to develop reliable models for design and operational considerations. A key element of the system is the interface between transportation and storage, namely the injection well, where various transient scenarios involving multiphase flow will occur.

In the literature there are very few data relevant for validation of vertical multiphase flow models for CO_2. Hence in this work, we present measurements of liquid holdup, pressure drop and flow regime for upward and downward flow of CO_2 in a pipe of inner diameter 44mm at a pressure of 6.5MPa, a condition relevant for CO_2-injection wells.

The experimental results indicate that the flow is close to no-slip. We have compared the experimental data to predictions by well-known models for phase slip and frictional pressure drop, and the results show that overall, the best model is the simplest one – the fully homogeneous approach, in which no slip is assumed and the friction is calculated simply by employing gas-liquid mixture properties in the single-phase friction model.

1. Introduction

CO_2 capture and storage (CCS) is seen as one of the technologies that are necessary to help mitigate climate change (Edenhofer et al., 2014). In order for CCS to attain the scale required to do so, full-scale deployment must commence and be scaled up such that by the mid century, several gigatonnes of CO_2 are captured each year (IEA, 2017). This CO_2 must be transported from the capture plants to the storage sites. In order to design and operate the CO_2 transportation and injection systems in a safe and efficient way, there is a need for flow models describing single- and multi-phase flow of CO_2 and CO_2-rich mixtures (Munkejord et al., 2016). CO_2 flows in pipes or tubes are also relevant in other applications, such as heat-pumping systems (Lorentzen, 1994; Pettersen et al., 2000), Brayton or Rankine cycles (Ayub et al., 2020), nuclear reactors (Eter et al., 2017) and heat storage (Ayachi et al., 2016).

The injection well constitutes the interface between the CO_2 storage and the transportation system. It is important to be able to predict the flow behaviour of the CO_2 both during normal operation, and during start-up, shut-in or undesired events like blow-outs. During normal operation, transients can be expected due to fluctuations in the CO_2 supply (Moe et al., 2020), due to batch-wise offshore delivery from ships (Aursand et al., 2017; Munkejord et al., 2020), or during injection into depleted natural-gas reservoirs (Sacconi and Mahgerefteh, 2020). Among other things, resulting temperature fluctuations could affect well integrity (Aursand et al., 2017).

Depending on the maximum allowable pressure in the CO_2 reservoir and other operational conditions, the CO_2 could be in a two-phase state in part of the well (see e.g. Munkejord et al., 2013). This was also the case for the CO_2-production well studied by Cronshaw et al. (1982). CO_2 has significantly different thermophysical properties compared to those of e.g. oil and natural gas. Therefore, existing models, validated for such fluids, may not be accurate for CO_2, and experimental validation is required. However, very few data are available in the literature for the vertical two-phase flow of CO_2 in relevant configurations. Cronshaw et al. (1982) presented temperature and pressure measured at several locations in a CO_2-production well for varying flow rates. In the upper part of the well, the CO_2-rich mixture includ-

* Corresponding author.
E-mail address: svend.t.munkejord@sintef.no (S.T. Munkejord).

https://doi.org/10.1016/j.ijmultiphaseflow.2021.103590

Nomenclature

C	Dimensionless pressure gradient, 1
d	Diameter, m
e	Specific internal energy, J kg^{-1}
$\hat{e}$	Total specific energy, J kg^{-1}
f	(Darcy) friction factor, 1
Fr	Froude number, 1
$\mathcal{F}$	Friction force, N m^{-3}
g_x	Gravitational acceleration in axial direction, m^{-3}
h	Specific enthalpy, J kg^{-1}
j	Volumetric flux, m s^{-1}
$\dot{m}$	Mass flux, kg m^{-2} s^{-1}
n	Number of experimental measurements, 1
P	Pressure, Pa
$\mathcal{Q}$	Heat flux per volume, W m^{-3}
Re	Reynolds number, 1
t	Time, s
u	Velocity, m s^{-1}
x	Axial coordinate, m
x	Gas mass fraction based on the mass fluxes, (5), kg kg^{-1}
y	Elevation, m
α	Volume fraction, m^3 m^{-3}
δ_{rms}	Root-mean-square deviation, (13)
σ	Surface tension, N m^{-1}
μ	Dynamic viscosity, kg m^{-1} s^{-1}
Φ	Coefficient in (6), 1
ρ	(Mass) density, kg m^{-3}
d	Drift
f	Friction
g	Gas
k	Phase k
ℓ	Liquid
m	Multiphase mixture
CCS	CO_2 capture and storage
EOS	Equation of state
IFE	Institute for Energy Technology
RMS	Root mean square

ing water was in a gas-liquid or gas-liquid-liquid multiphase state, although the gas fraction was not measured. Some field data can be found for CO_2 wells (see Lu and Connell, 2014; Li et al., 2017). These data are less detailed than desirable for flow model validation.

In principle, the complicated topology of two-phase flows can be simulated in detail using front-capturing (Osher and Fedkiw, 2001; Sethian, 2001) or front-tracking (Tryggvason et al., 2001) methods. However, due to the computational intensity, such methods can only be used on relatively small computational domains. Therefore one resorts to considering an average of the two-phase flow, not resolving the full details of the interfaces (Stewart and Wendroff, 1984; Drew and Passman, 1999). Even in this case, when complicated equations of state are involved, three-dimensional simulations are limited to small domains (Gjennestad et al., 2017). As a result, for engineering purposes, two- (or multi-) phase flows in pipes and wells are commonly described using one-dimensional models. The most general approach is usually referred to as the two-fluid model (Stewart and Wendroff, 1984). Herein, the difference between the gas and liquid velocity is determined through inter-phasic friction models, the development of which involves extensive use of experimental data. For several flow regimes, it is possible to correlate the relative velocity between the phases, the *slip velocity*, as a function of the flow variables (Zuber and Findlay, 1965; Ishii, 1977; Hibiki and Ishii, 2002). This a priori knowledge of the flow can be employed to reduce the number of transport equations to be solved, and the result is called the *drift-flux model*. In particular, drift-flux models have been developed for two- and three-phase flows in wells (Shi et al., 2005b; 2005a). In addition to slip models, models for the *frictional pressure drop* are needed in order to perform simulations. Friction models for two-phase flow exist in various forms, ranging from empirical (Beggs and Brill, 1973) to phenomenological models describing the characteristic features of different flow regimes (RELAP5 Development Team, 1995). See also the review in Dorao et al. (2019).

In the present work, we address the lack of vertical experimental data for two-phase flow of CO_2. We employ an experimental setup designed to generate liquid holdup and pressure-drop data, along with flow-regime information, during steady-state operation (Håvelsrud, 2012; Farokhpoor et al., 2020). A data series has been generated for varying gas and liquid fluxes of pure CO_2, both upwards and downwards, at a pressure of 6.5MPa. This pressure has been chosen since it is relatively close to the critical pressure (7.38MPa), while at the same time giving a state that is clearly two-phase. As described in the following, this has allowed us to compare slip models and frictional pressure-drop models from the literature with experimental data, giving guidance to modellers wanting to describe the flow of CO_2 in wells.

2. Experimental setup

Vertical up-flow and down-flow experimental data have been acquired for two-phase pure CO_2 saturated at 6.5MPa in FALCON, IFE's flow assurance loop for CO_2 transport. The corresponding saturation temperature is 24.4°C. The main pipe of the flow loop has an inner diameter of 44mm, a length of 13.7m and an effective surface roughness estimated to be 17m, giving a relative pipe roughness of 3.9×10^{-4} relevant for friction calculations. The experimental setup is described by Farokhpoor et al. (2020), who studied horizontal and near horizontal flow of CO_2. Schematic drawings of the test facility's overall design and the instrumentation of the test section, for vertical pipe configurations, are shown in Fig. 1.

The temperature is controlled by a combined heating/cooling system where a coolant is circulated in copper-tubing-type heat exchangers 'coiled' on to the main separator and the test section. The coolant temperature is tuned so that the heat transfer to the system, via the heat exchangers, just balance the heat added by the pumps and the heat loss to the ambient, justifying the assumption of an adiabatic system. In this way the temperature/pressure is controlled in a stable and accurate way. The net heat loss, or gain, depends on the pumps' rotational speed (i.e., the flow rates), the operating temperature and the ambient temperature (heat loss/gain). The temperature of the coolant is controlled by combined heating and cooling. The effect of the electrical heater and the cooling plant enables stable operating temperatures in the range −10°C to 40°C if the ambient temperature is around 10°C. All pipes and vessels are well insulated.

The main differences between the up-flow and down-flow configurations are the position of the broad-beam gamma densitometer and the inlet and outlet sections. A pre-separator is included in the vertical-down setup and the inlet merger is Y-shaped. In the vertical-up setup, there is no outlet pre-separator, only the Y-split, and the inlet merger is a joint of two half-circles made by steel tubes, see Fig. 1 for an outline. The gas and liquid phases are drawn from, respectively, the top and the bottom of the main separator and conveyed as single-phase fluids, in separate feed lines, to the inlet merger of the test section. From a view cell on the liquid feed line, we can observe that no bubbles are present in the liquid, i.e., no boiling has taken place. From temperature mea-

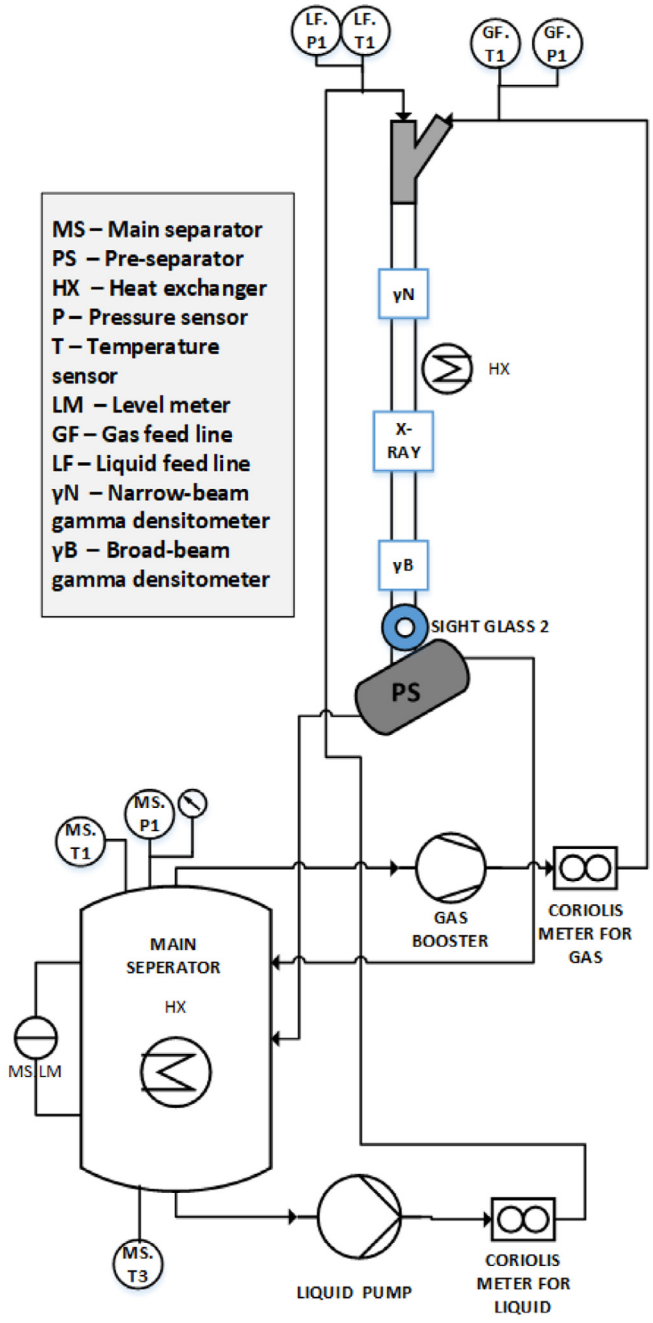

(a) Process design layout for vertical downward flow with indication of the gamma densitometers and X-ray locations,

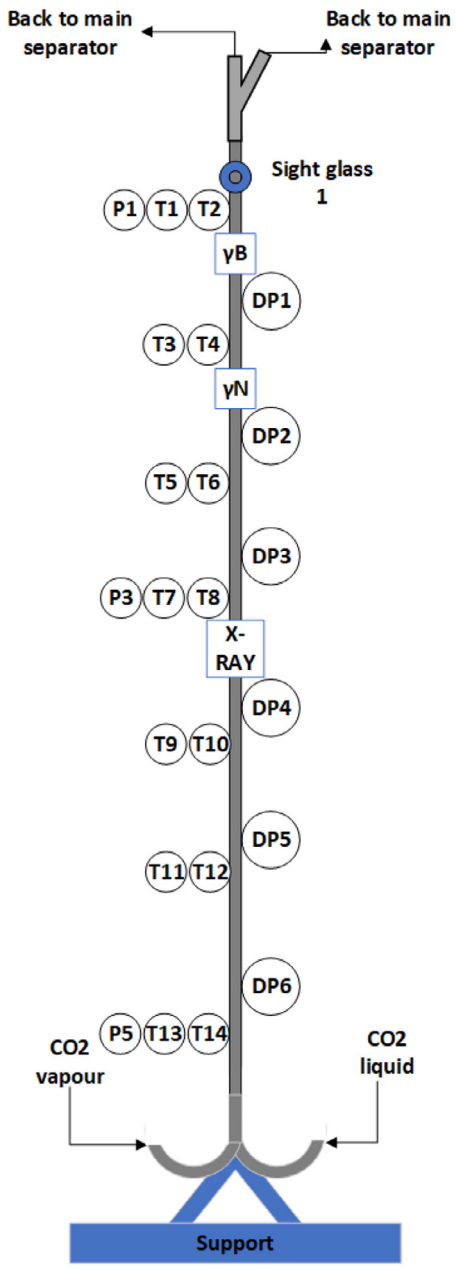

(b) Instrumentation of the test pipe for vertical upward experiments with indication of instrument locations.

Fig. 1. Schematic of the FALCON test facility located at the Institute for Energy Technology (IFE).

surements just upstream of the merger, we can also verify that both fluid phases have temperatures that closely correspond to the vapour-liquid equilibrium line. This means that no flashing or condensation should take place when the gas and liquid streams are merged.

The objective of the experimental campaign was threefold, namely, to measure the pressure drop, to measure the liquid holdup, and to detect the flow regime at different volumetric phase fluxes. The liquid holdup was measured using a broad-beam γ-densitometer and a single camera X-ray setup. From the measured holdup, the phase slip factor (u_g/u_ℓ) can be calculated. A narrow-beam γ-densitometer is included in the flow loop setup, giving supplementary information on the liquid holdup, primarily used to evaluate the flow development. Using the X-ray results and images from a high-speed camera, visualizing the flow through a sight glass, the flow regimes were manually determined. The overall pressure drop was determined by averaging measurements from six piezoresistive differential pressure sensors. With the liquid holdup measured by the X-ray system as input, the overall pressure drop was split in a hydrostatic and friction contribution using densities predicted by the Span and Wagner (1996) equation of state (EOS).

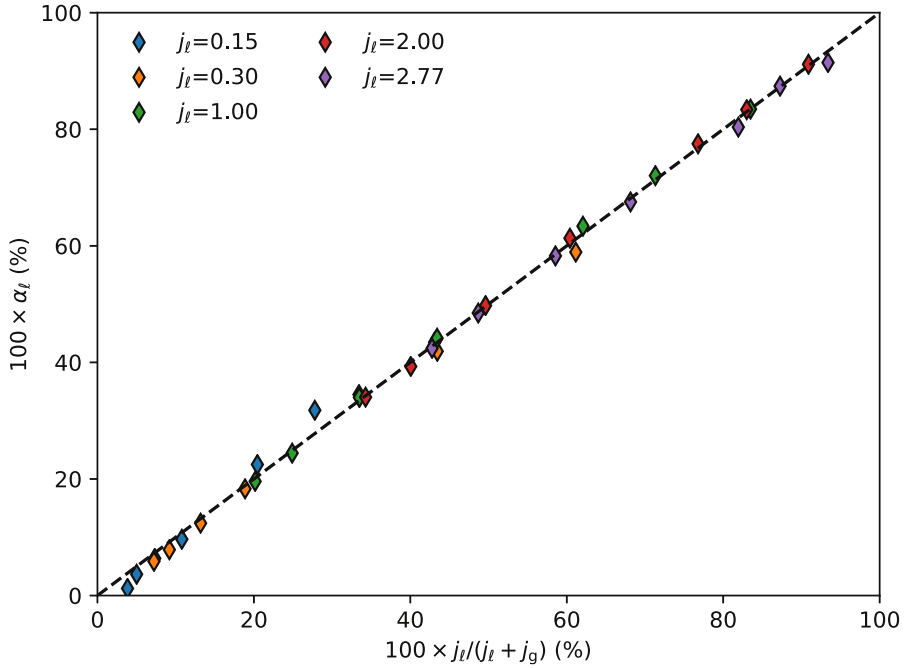

Fig. 2. Measured holdup plotted versus homogeneous holdup for the upward flow experiments.

Table 1
Estimated measurement uncertainties in input and measured data.

Property	Type	Uncertainty
Pipe diameter	Absolute	± 0.1mm
Absolute pressure	Relative	± 1.5%
Delta pressure	Relative	± 7%
Temperature	Absolute	± 1.0°C
Liquid holdup – Broad-beam γ-meter	Absolute	± 0.02
Liquid holdup – Narrow-beam γ-meter	-	± 0.035
Liquid holdup – X-ray system	Absolute	± 0.03
Liquid volumetric flux	Relative	± 4%
Gas volumetric flux	Relative	± 3%

In addition to the geometry (upward or downward flow), the main experimental parameters are the volumetric gas flux, j_g, and volumetric liquid flux, j_ℓ. The test matrix consisted of all combinations of $j_g \in \{0.2, 0.4, 0.6, 1.3, 2.0, 3.0, 4.0\}$ m s^{-1}, and $j_\ell \in \{0.15, 0.3, 1.0, 2.0, 3.0\}$ m s^{-1}. The phase mass flows are measured using Coriolis flow meters, and volumetric fluxes are calculated from density estimates.

The critical pressure of CO_2 is 73.8bar, and since the pressure in the experiments is relatively close to that, the gas and liquid thermophysical properties are similar. The liquid-to-gas density ratio is $\rho_\ell/\rho_g = 2.83$ while the viscosity ratio is about the same; $\mu_\ell/\mu_g = 2.75$. The surface tension at this pressure is only approximately 0.5mNm^{-1}. The phase slip factor in these experiments is therefore expected to be close to one, $u_g/u_\ell \approx 1$.

The main experimental uncertainties are listed in Table 1, and they have been estimated following the ISO Guide to the expression of uncertainty in measurement (Joint Committee for Guides in Metrology, 2008). The uncertainty in the measurements (flow stability, data acquisition, etc.) is handled as a Type A standard uncertainty with normal distribution of data, while instrument accuracies (datasheets, previous experience, calibrations, inter-comparisons, etc.) are handled as Type B standard uncertainties, with rectangular distribution. A coverage factor of 2 has been used to get 95% confidence. For the flow rates, the contribution from Type A and Type B to the combined uncertainty varies with the magnitude of the flow rates. For the pressure and differential pressures, Type B dominates over Type A in the combined uncertainties. The holdup uncertainties are based on calibrations and long term experience, while the temperature uncertainties are based on the sensor accuracy and comparisons with redundant sensors.

3. Models

Since, in this work, we study vertical two-phase flow where the two phases have relatively similar thermophysical properties, the key models for simulation purposes are those for friction and phase slip, in addition to the property models, which we briefly discuss in the following.

One-dimensional single-component two-phase flow with equilibrium in pressure, temperature and chemical potential can be described by mass conservation and momentum and energy balance equations as follows.

$$\frac{\partial}{\partial t}\left(\sum_k \alpha_k \rho_k\right) + \frac{\partial}{\partial x}\left(\sum_k \alpha_k \rho_k u_k\right) = 0, \tag{1}$$

$$\frac{\partial}{\partial t}\left(\sum_k \alpha_k \rho_k u_k\right) + \frac{\partial}{\partial x}\left(\sum_k \alpha_k \rho_k u_k^2\right) + \frac{\partial P}{\partial x} = \rho_m g_x - \mathcal{F}, \tag{2}$$

$$\frac{\partial}{\partial t}\left(\sum_k \alpha_k \rho_k \hat{e}_k\right) + \frac{\partial}{\partial x}\left(\sum_k \alpha_k \rho_k u_k (h_k + 1/2u_k^2 + gy)\right) = \mathcal{Q}. \tag{3}$$

Herein, α_k is the volume fraction of phase k and ρ denotes density, P denotes pressure and u is the velocity. The total specific energy includes the internal, kinetic and potential energy; $\hat{e}_k = e_k + 1/2u_k^2 + gy$, where g is the gravitational acceleration and y is the elevation. In the momentum equation, g_x is in the axial direction of the pipe.

The enthalpy is $h_k = e_k + P/\rho_k$. The subscript m denotes (multiphase) mixture quantities. For example, the mixture density is $\rho_m = \sum_k \alpha_k \rho_k$. $\mathcal{Q}$ is the heat flux transferred to the fluid through the pipe wall and $\mathcal{F}$ is the wall friction. In this work, we will assume adiabatic flow, $\mathcal{Q} = 0$.

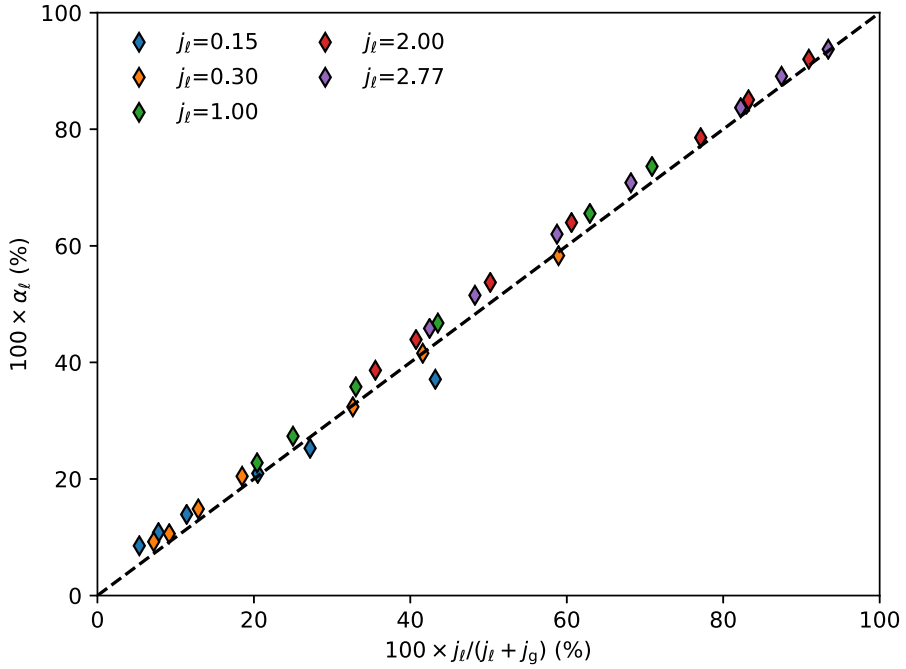

Fig. 3. Measured holdup plotted versus homogeneous holdup for the downward flow experiments.

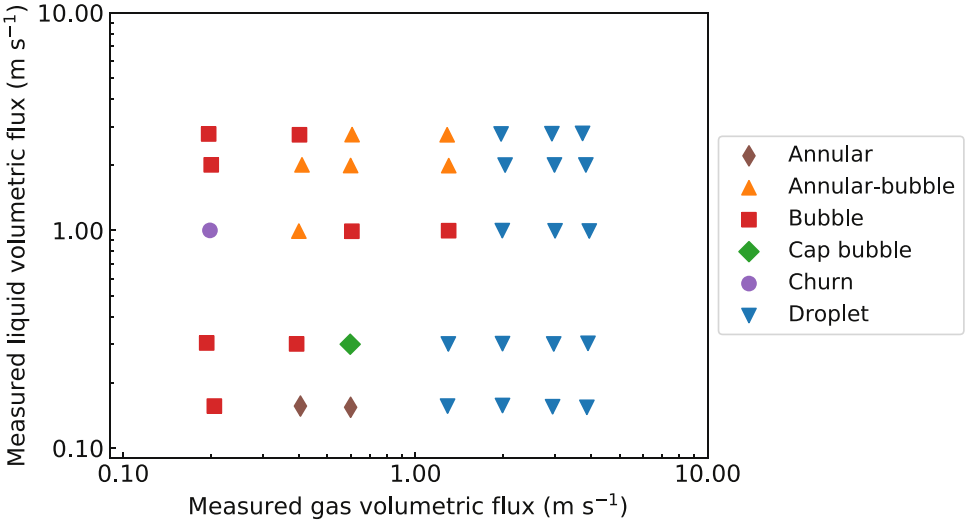

Fig. 4. Flow regime observed in experiments with upward flow.

In addition to the above equations, to close the system, one needs a slip relation, i.e., a model for the difference between the phasic velocities, and an equation of state.

3.1. Friction models

For single-phase flow, the wall friction, $\mathcal{F}$, is commonly calculated as

$$\mathcal{F} = f_k \frac{\dot{m}|\dot{m}|}{2\rho_k d}, \tag{4}$$

where f_k is the Darcy friction factor, $\dot{m} = \rho u$ is the mass flux, and d is the inner pipe diameter.

Two-phase friction models can be classified based on assumptions and modelling approach (see Collier and Thome, 1994; Hewitt, 2011). The simplest approach is that of the homogeneous model, where the phases are assumed to be well mixed so they can be treated as a single phase, and the friction can be described using a friction factor obtained from the Reynolds number based on the gas-liquid mixture properties – essentially replacing k by m in (4). Here, the Reynolds number is calculated using a mass-based harmonic average of the phase viscosities,

$$\frac{1}{\mu_\mathrm{m}} = \frac{x}{\mu_\mathrm{g}} + \frac{1-x}{\mu_\ell}, \tag{5}$$

where x denotes the gas mass fraction based on the mass fluxes.

Several empirical modifications to obtain a two-phase friction factor have been suggested. One commonly used model is the Beggs and Brill (1973) correlation, which employs correction factors to the single-phase no-slip friction factor based on flow regime and inclination.

Another main approach is that of separated flow, i.e., where the gas and liquid flow are accounted for separately, each with its own velocity and area fraction of the channel cross section. Here, the

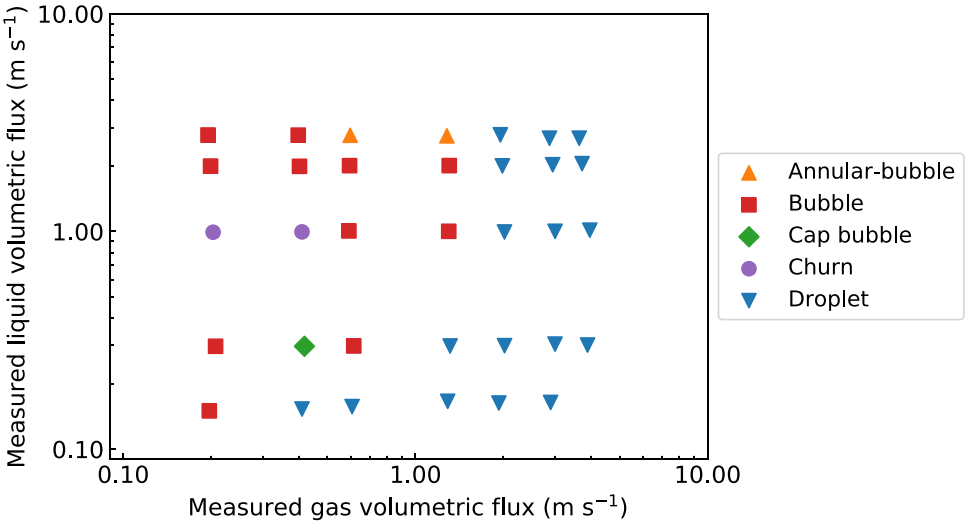

Fig. 5. Flow regime observed in experiments with downward flow.

wall friction is often modelled as

$$\mathcal{F} = f_\ell \frac{\dot{m}|\dot{m}|}{2\rho_\ell d}\Phi, \tag{6}$$

where ℓ denotes the liquid phase and Φ is a two-phase friction multiplier. One commonly used separated-flow friction model is that of Friedel (1979).

In principle, more accurate friction predictions can be achieved using phenomenological models, where the flow regime is identified, and separate adapted models are applied accordingly. The friction model employed in the RELAP5 model is one example (RELAP5 Development Team, 1995), but will not be further evaluated in this work.

All friction models will require the calculation of single-phase friction factors based on Reynolds number and relative pipe roughness. In this work we will, as default, use the explicit formula of Haaland (1983) to calculate the Darcy friction factor, instead of iteratively solving the more accurate Colebrook-White equation (see e.g. White, 1994).

3.2. Drift-flux models

The basic idea of drift-flux modelling is that the gas velocity, u_g, can be related to the volumetric flux, $j = \alpha_g u_g + \alpha_\ell u_\ell$, of the mixture and a drift velocity, u_{gd}, taking into account the difference between the mixture flux and the gas velocity, including the buoyancy effect. The drift-flux concept was first introduced by Zuber and Findlay (1965) for 1D flow, and due to its simplicity, many correlations have been developed for predictions of phase slip and holdup in two- and three-phase flow.

The gas velocity correlation in the drift-flux formalism is usually given as

$$u_g = C_0 j + u_{gd}, \tag{7}$$

where the profile parameter C_0 correlates the effect of cross-sectional velocity and holdup profile information, and u_{gd} is the drift velocity describing the local phase slip. According to Zuber and Findlay (1965), $1.0 \le C_0 \le 1.5$. In our simulation code, the u_{gd} term is implemented such that it gives a positive contribution against gravity.

In this work, we evaluate three different slip models. First, we have implemented the Zuber and Findlay (1965) model for the churn-turbulent bubbly regime,

$$u_g = 1.18 j + 1.53\left[\frac{\sigma g \Delta\rho}{\rho_\ell^2}\right]^{1/4}. \tag{8}$$

Herein σ is the surface tension and $\Delta\rho = \rho_\ell - \rho_g$.

Second, we consider the model of Shi et al. (2005b), which was developed for vertical to near horizontal flow of oil/gas/water based on experimental data from large-diameter pipes. The third model included is the one of Pan et al. (2011a,b), which is an adaptation of the Shi et al. (2005b) model for CO_2 flow in wells. Here, we label this model T2Well.

3.3. Dimensionless parameters

For vertical multiphase flows, the Froude number, relating inertia to gravity, is a significant parameter. Several formulations are possible. Here we use

$$Fr_m = \frac{u_m^2}{gd}, \tag{9}$$

where $u_m = \dot{m}/\rho_m$ is the mass-weighted mixture velocity. In this subsection, the mixture properties are calculated using volume fractions for homogeneous (no-slip) flow. This definition is employed in the Friedel (1979) and Beggs and Brill (1973) correlations. At times a density-dependent prefactor is included in the Froude number for multiphase flows, see e.g. Farokhpoor et al. (2020). Since in the present experiments the gas and liquid densities are almost constant, such a prefactor is not included here.

A multitude of different Reynolds numbers are in use for multiphase flows. The Friedel (1979) correlation employs a gas-only and a liquid-only Reynolds number, calculated assuming that the whole mass flow is gas, and liquid, respectively. In the Beggs and Brill (1973) correlation and in the homogeneous model, the two-phase mixture Reynolds number is calculated as

$$Re_m = \frac{\rho_m u_m d}{\mu_m}, \tag{10}$$

although with the difference that in the homogeneous model, we employ the relation (5) for the two-phase mixture viscosity, whereas in Beggs and Brill (1973), a volume average of the phasic viscosities is used. It is also common to calculate gas and liquid Reynolds numbers based on the volumetric fluxes,

$$\tilde{Re}_k = \frac{\rho_k j_k d}{\mu_k}. \tag{11}$$

In the present experiments, we have $Re_m \in \{1.9 \times 10^5 \ldots 3.6 \times 10^6\}$, $\tilde{Re}_g \in \{1.0 \times 10^5 \ldots 2.2 \times 10^6\}$, $\tilde{Re}_\ell \in \{8.4 \times 10^4 \ldots 1.6 \times 10^6\}$.

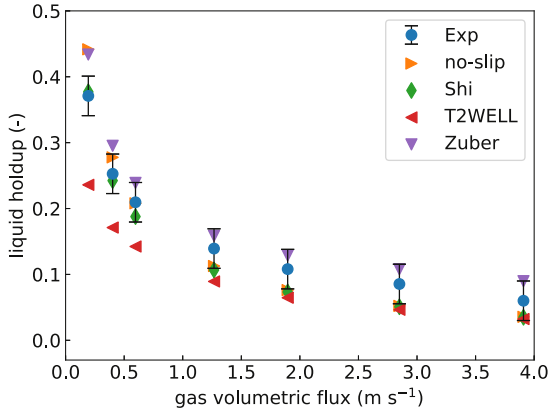

(a) $j_\ell = 0.15\,\mathrm{m\,s^{-1}}$.

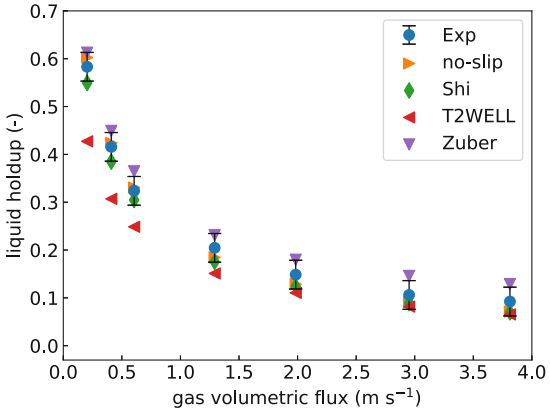

(b) $j_\ell = 0.30\,\mathrm{m\,s^{-1}}$.

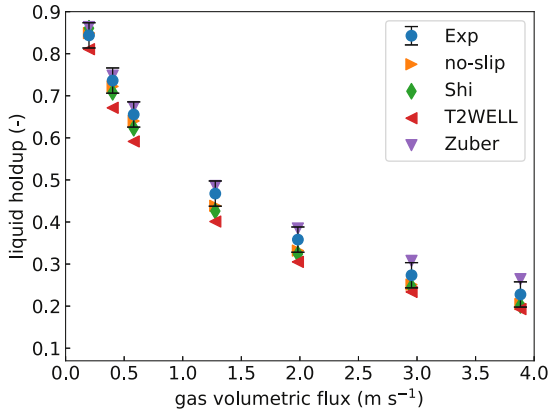

(c) $j_\ell = 1.00\,\mathrm{m\,s^{-1}}$.

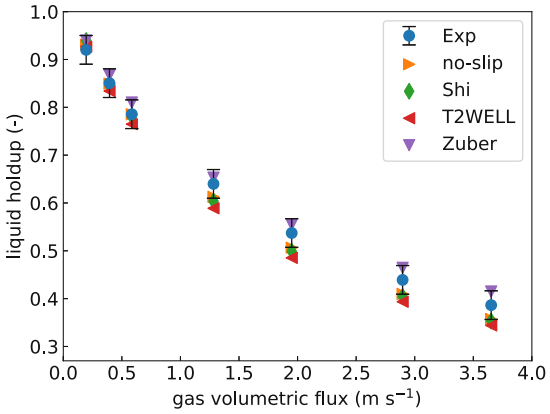

(d) $j_\ell = 2.00\,\mathrm{m\,s^{-1}}$.

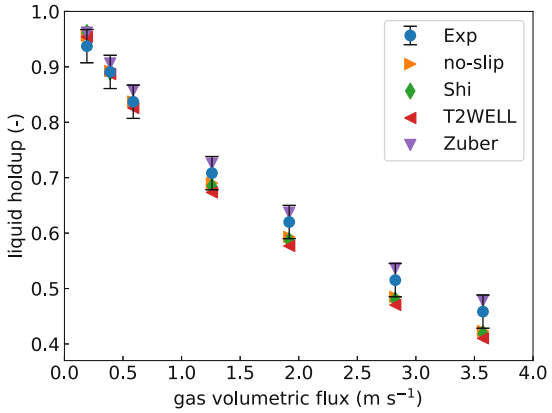

(e) $j_\ell = 2.77\,\mathrm{m\,s^{-1}}$.

Fig. 6. Downward flow: Measured and calculated liquid holdup, α_ℓ, as a function of gas volumetric flux, j_g, for varying liquid volumetric flux, j_ℓ.

The experimental pressure gradient data can be normalized by the dynamic pressure based on the mixture velocity and density as follows.

$$C = \frac{\left|\frac{\Delta P}{\Delta x}\right| d}{\frac{1}{2}\rho_m u_m^2}. \tag{12}$$

This definition will be employed in Section 4.4.

3.4. Thermophysical property models

In this work, the highly accurate Helmholtz-type equation of state (EOS) of Span and Wagner (1996) for CO_2 has been used. The EOS is used to calculate what phases are stable, and the densities and energies of the existing phases.

The viscosity of pure CO_2 for conditions relevant for transport and capture is described using the correlation of Fenghour et al. (1998) to an accuracy below 2%. The thermal

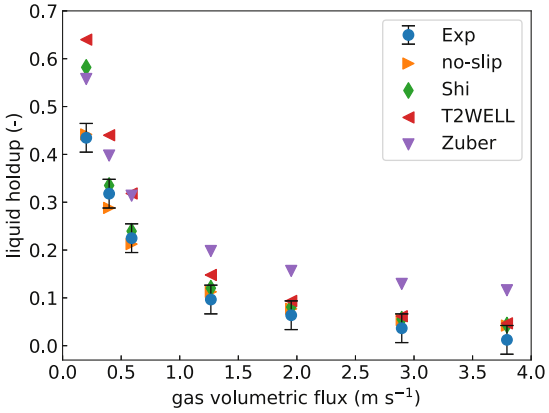

(a) $j_\ell = 0.15\,\mathrm{m\,s^{-1}}$.

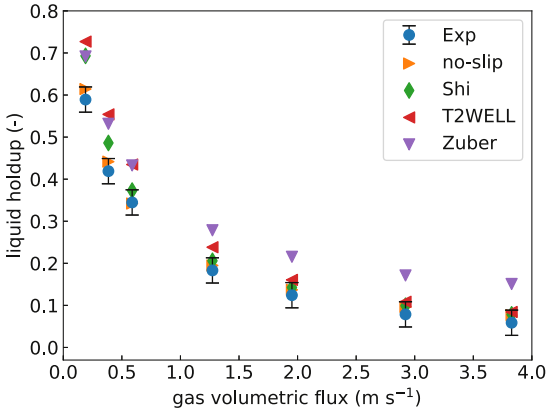

(b) $j_\ell = 0.30\,\mathrm{m\,s^{-1}}$.

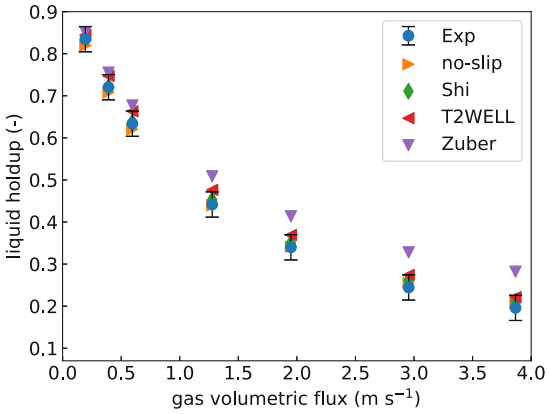

(c) $j_\ell = 1.00\,\mathrm{m\,s^{-1}}$.

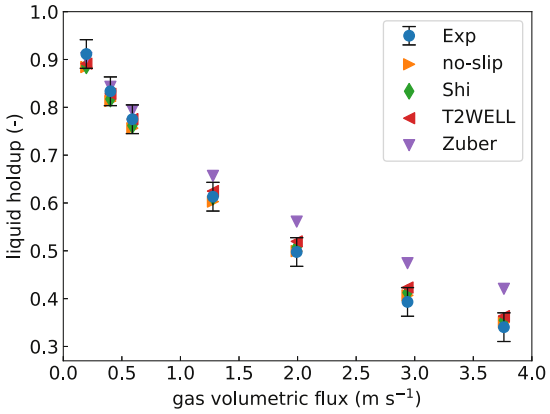

(d) $j_\ell = 2.00\,\mathrm{m\,s^{-1}}$.

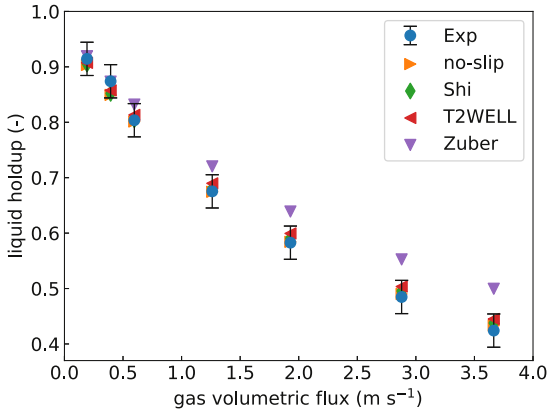

(e) $j_\ell = 2.77\,\mathrm{m\,s^{-1}}$.

Fig. 7. Upward flow: Measured and calculated liquid holdup, α_ℓ, as a function of gas volumetric flux, j_g, for varying liquid volumetric flux, j_ℓ.

conductivity of pure CO_2 is correlated to a similar degree of accuracy by Vesovic et al. (1990). The gas-liquid interfacial surface tension is modelled using the correlation of Rathjen and Straub (1977).

For the flash calculations, we utilize our framework for calculation of thermodynamic properties (Wilhelmsen et al., 2017; Hammer et al., 2020). The framework interface the TREND thermodynamics library (Span et al., 2016) for the Helmholtz EOS.

3.5. 1D fluid flow simulator

The non-linear system of governing equations for the flow (1)–(3) are discretized on a regular forward-staggered grid us-

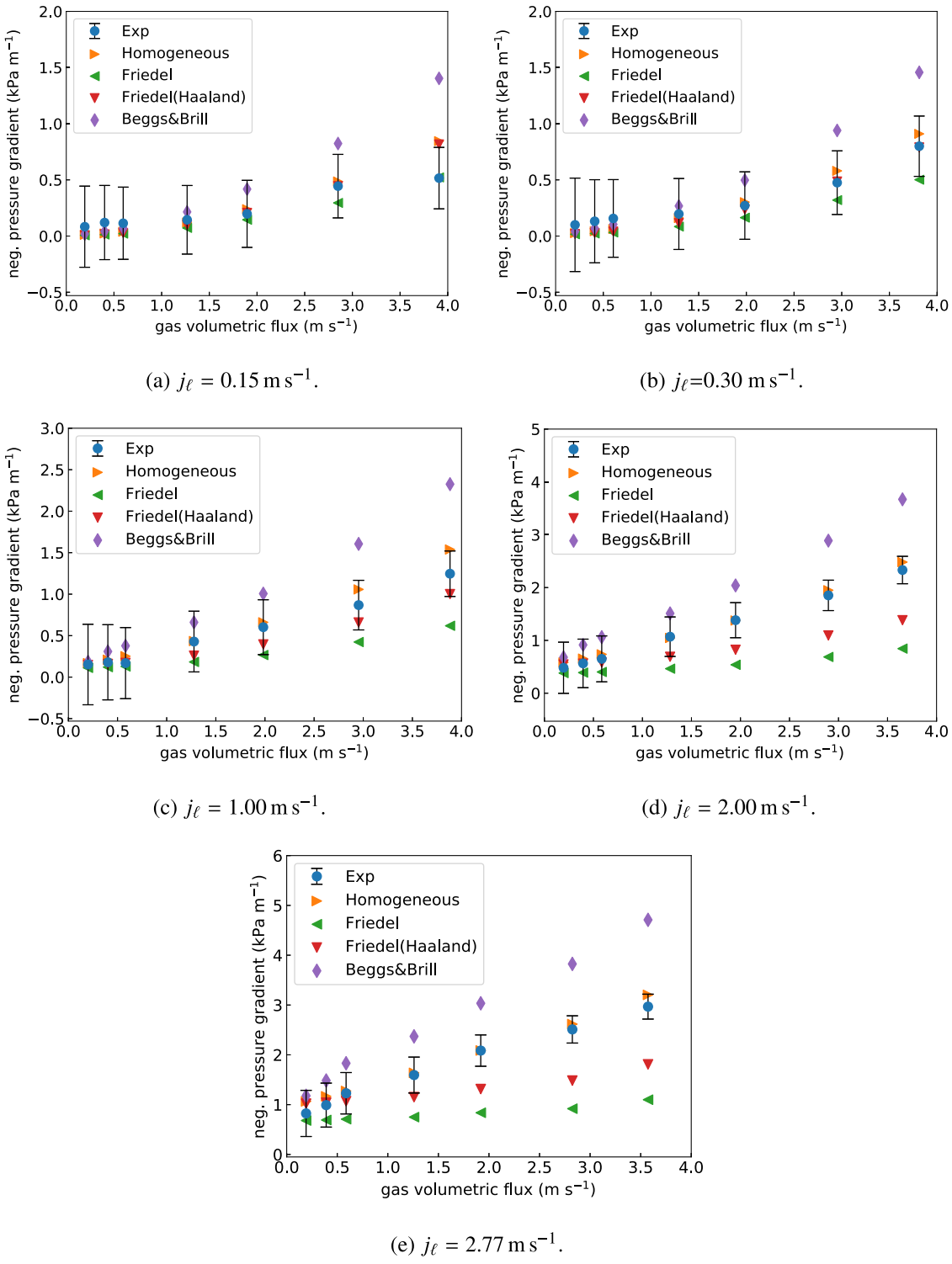

(a) $j_\ell = 0.15\,\mathrm{m\,s^{-1}}$. (b) j_ℓ=0.30 $\mathrm{m\,s^{-1}}$.

(c) $j_\ell = 1.00\,\mathrm{m\,s^{-1}}$. (d) $j_\ell = 2.00\,\mathrm{m\,s^{-1}}$.

(e) $j_\ell = 2.77\,\mathrm{m\,s^{-1}}$.

Fig. 8. Downward flow: Measured and calculated negative frictional pressure gradient as a function of gas volumetric flux, j_g, for varying liquid volumetric flux, j_ℓ.

ing a first-order upwind-type finite-volume method similar to the one discussed by Zou et al. (2016). The resulting discrete equation system is solved by a Jacobian-free Newton–Krylov method as discussed by Knoll and Keyes (2004). Here we employ the PETSc library (Balay et al., 1997; 2018) using the `SNESNEWTONLS` method, which is a Newton-based nonlinear solver that uses a line search. Within this method, the BiCGStab (stabilized version of bi-conjugate gradient) method with SOR (successive over-relaxation) as a preconditioner is employed. Further details on the model and methods can be found in Munkejord et al. (2020).

To obtain the results presented in the following, we employed a grid of 20 cells, running the simulations for 200s to arrive at the steady-state solution.

4. Results and discussion

In the following we will present our experimental data relevant for CO_2 well flow, and compare experimental results to the models for friction and slip presented in Section 3.

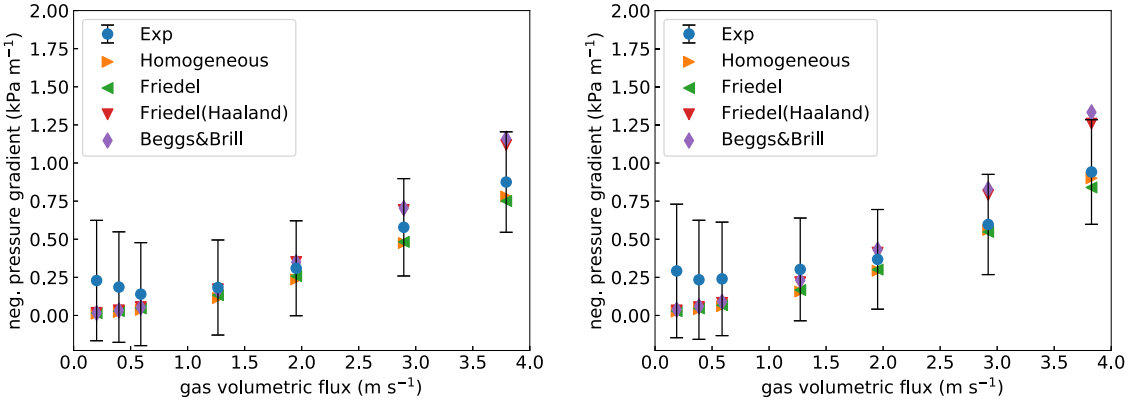

(a) $j_\ell = 0.15\,\mathrm{m\,s^{-1}}$. (b) $j_\ell = 0.30\,\mathrm{m\,s^{-1}}$.

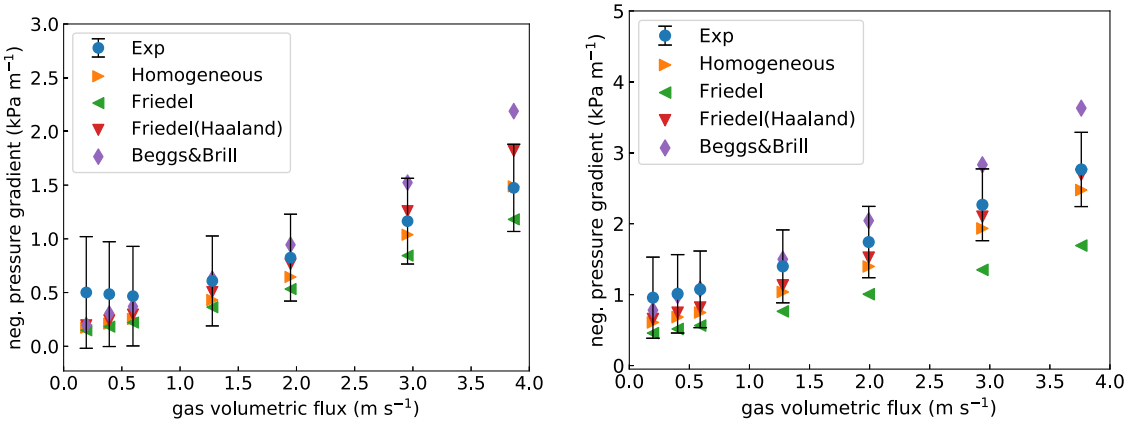

(c) $j_\ell = 1.00\,\mathrm{m\,s^{-1}}$. (d) $j_\ell = 2.00\,\mathrm{m\,s^{-1}}$.

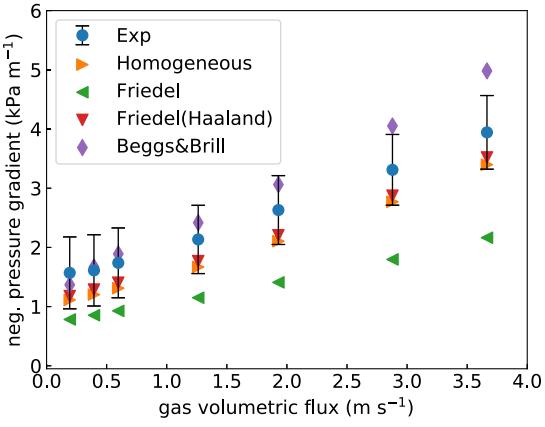

(e) $j_\ell = 2.77\,\mathrm{m\,s^{-1}}$.

Fig. 9. Upward flow: Measured and calculated negative frictional pressure gradient as a function of gas volumetric flux, j_g, for varying liquid volumetric flux, j_ℓ.

4.1. Experimental data

4.1.1. Liquid holdup

In Fig. 2, we have plotted the measured holdup, based on the X-ray system, against the homogeneous holdup for the upward flow geometry. The homogeneous holdup is simply the fraction of the liquid volumetric flux to the total volumetric flux in each experiment. From this plot we can get qualitative information regarding phase slip. If the gas velocity is larger than the liquid velocity, the measured holdup will be larger than the input homogeneous holdup, and the experimental data points will lie to the left of the dashed no-slip line. The figure shows that except for the experiments with an inlet holdup less than 20%, for which gas accumulation and $u_\ell > u_g$ is registered, the flow is essentially no-slip. The experiments with low inlet liquid holdup will have a high relative uncertainty in the holdup measurements, as the measurement un-

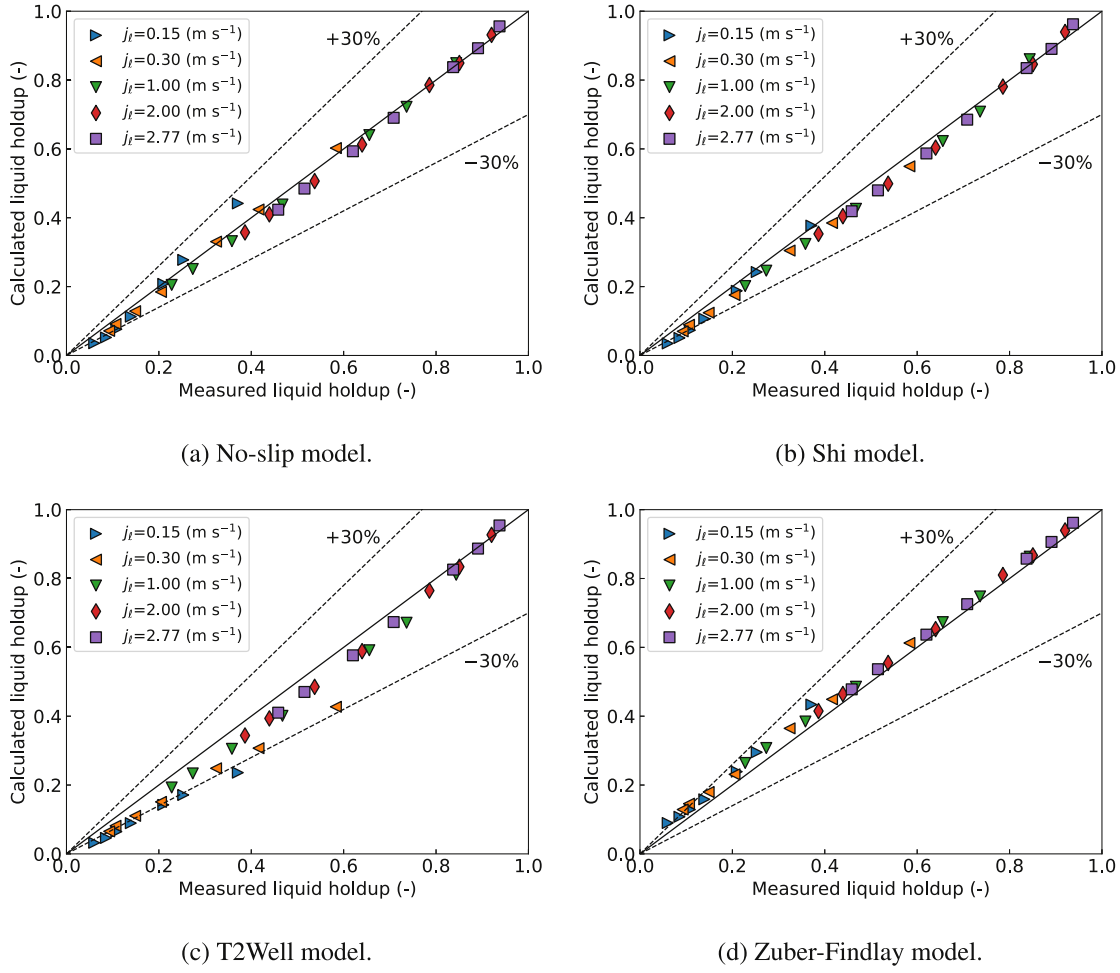

Fig. 10. Downward flow: Comparison between measured and computed liquid holdup for different slip models.

certainty is absolute, see Table 1. The experiments with an inlet holdup less than 20%, are therefore most likely also no-slip.

In Fig. 3, we have plotted the measured holdup, based on the X-ray system, against the homogeneous holdup for the downward flow geometry. The figure shows that except for 2–3 outliers, all experiments have liquid accumulation and $u_g > u_\ell$. As the liquid density is approximately 2.8 times the gas density, and the gravitational force would favour $u_\ell > u_g$, this is slightly surprising.

4.1.2. Flow regime

The flow regimes for these experiments are dominated by the gas and liquid phases being well mixed. The phases are observed to be segregated only to a very small extent. This is presumably because of the low density differences and low surface tensions. The following measurements are used to support the flow regime determination:

- holdup and $\delta p/\delta x$ time series, which will indicate intermittent flow behaviour
- the optical videos (very short recording time)
- X-ray projections of phase distribution (27 seconds side view projections)

Since there was very little intermittency in the flow and the videos were to limited help, the flow regime findings are mainly based on the X-ray projections. It must be admitted that the flow regimes are encumbered with significant uncertainties and that they involve guesswork.

The flow regime map identified for the upward flow is shown in Fig. 4, and the flow regime map for downward flow is shown in Fig. 5. A qualitative description of the flow regimes is given in Table 2. In both figures, we see gas-continuous flow with entrained liquid droplets/drops at high volumetric gas flux. For low volumetric gas flux, the flow is mostly liquid continuous or a chaotic gas-liquid mixture. Some points also indicate segregated annular flow, but there is no clearly defined annular region in the flow-regime maps.

4.2. Comparison of experimental data and calculated results

To evaluate slip and friction models, our dynamic 1D flow simulator, Section 3.5, was configured to match the experimental flow geometries and simulated to steady state. As boundary conditions for the simulations, the mass flow for each phase was specified at the inlet and the pressure was specified at the outlet. The pipe was initialized with a saturated state defined by the exit pressure, with a homogeneous flow based on the inlet condition. The pipe was considered to be adiabatic.

In this work, we have tested four models for pipe friction, as tabulated in Table 3. The original Friedel (1979) correlation includes an explicit equation for the friction factor that does not include the effect of pipe roughness. As the relative surface roughness in the experimental setup is high, it was deemed relevant to use the Friedel correlation with both the original friction factor model and the Haaland model.

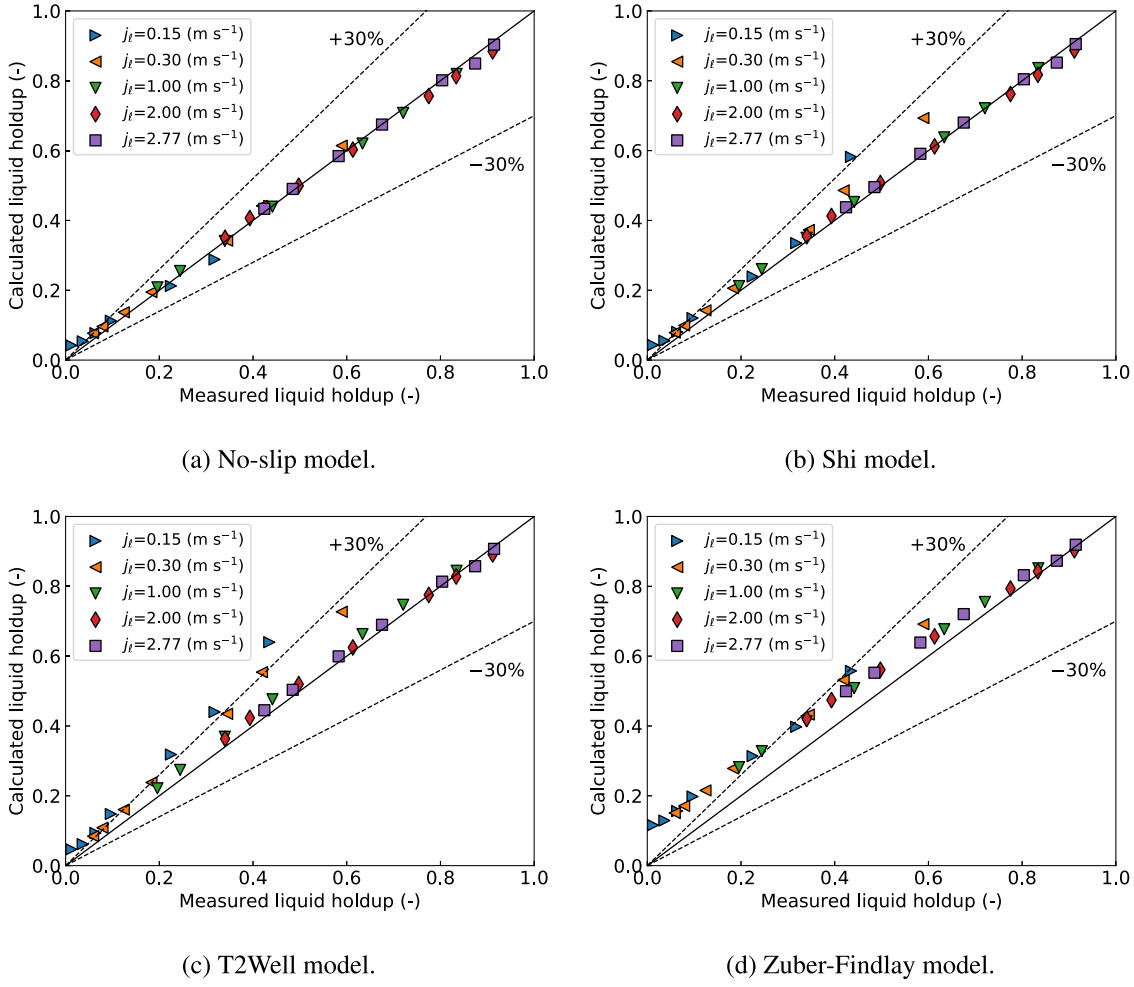

Fig. 11. Upward flow: Comparison between measured and computed liquid holdup for different slip models.

Table 2
Flow regime description.

Flow regime	Description
Bubble	Liquid-continuous flow with entrained gas bubbles
Droplet	Gas-continuous flow with entrained liquid droplets/drops
Annular	Liquid-rich near the wall with a gas-rich core, not necessarily gas continuous
Annular-bubble	Little gas in the annular region near the wall, bubble flow in the centre
Cap bubble	Bubble flow where small bubbles have coalesced into larger cap bubbles
Churn	Bubble flow with larger, 'chaotic' gas structures

Table 3
Friction models considered.

Model	Description
Homogeneous	Friction calculated as for single-phase flow, using gas-liquid mixture properties.
Friedel	The Friedel (1979) friction model.
Friedel (Haaland)	Friedel (1979) correlation with Haaland (1983) friction factor.
Beggs & Brill	Two-phase friction factor correlation of Beggs and Brill (1973).

Further, we have tested four models for gas-liquid slip, as displayed in Table 4, where only the T2Well correlation is explicitly developed for CO_2 flow.

4.2.1. Liquid holdup vs. gas volumetric flux

This section presents the calculation results for the different slip models presented in Table 4. The frictional pressure drop is calculated by the Friedel (Haaland) correlation.

Fig. 6 presents the downward-flow measured and calculated liquid holdup as a function of gas volumetric flux, j_g, with error bands indicating the estimated experimental uncertainty. Each sub-figure is generated for an approximately constant liquid volumetric flux, j_ℓ. We observe that there is quite good agreement between models and experiments, but most of the models predict too low liquid holdup, which would correspond to an underprediction of the phase slip. The T2Well model is seen to underpredict the holdup for low volumetric fluxes, i.e., for j_ℓ at 0.3m s^{-1} or below

Table 4
Slip models considered.

Model	Description
no-slip	Homogeneous flow ($u_\ell = u_g$)
Shi	Drift-flux correlation flow of oil/gas/water based on large-pipe experimental data (Shi et al., 2005b).
T2Well	Adaption of Shi model for CO_2 well flow (Pan et al., 2011a,b).
Zuber	Equation (65) of Zuber and Findlay (1965). See Equation (8).

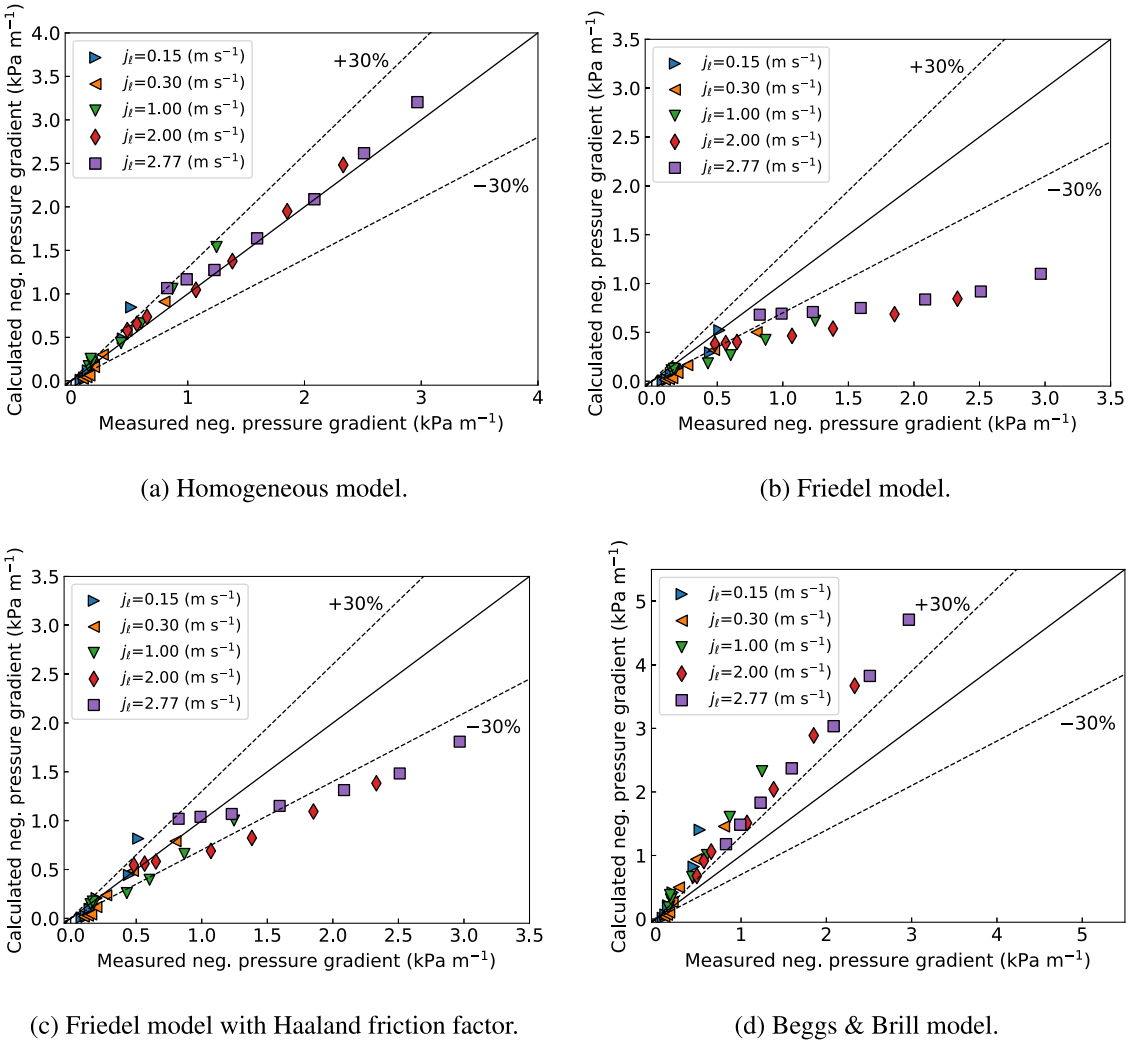

(a) Homogeneous model.

(b) Friedel model.

(c) Friedel model with Haaland friction factor.

(d) Beggs & Brill model.

Fig. 12. Downward flow: Comparison between measured and computed frictional pressure drop for different friction models.

and j_g below about 1.3m s^{-1}. The no-slip model, the Zuber-Findlay model and the Shi model have similar overall performance in this case, although Zuber-Findlay has a tendency to overprediction for high gas volumetric fluxes and the other models have a tendency to underprediction. The result is consistent with the fact that the measurements show some tendency towards 'liquid accumulation', and it indicates that the estimated drift velocity is low.

Fig. 7 shows the upward flow measured and calculated liquid holdup as a function of gas volumetric flux, j_g. We observe that the Zuber-Findlay model overpredicts the phase slip, consistently giving a too large liquid holdup. Given the qualitative results shown in Fig. 2, it is not surprising that the no-slip model gives the best fit with the experiments. The figure also shows an overprediction in holdup from both the Shi and the T2Well model. This is a result of those models predicting a larger slip ($u_g - u_\ell$) than what is the case in the experiment. For those models, the deviation is largest for low volumetric fluxes, i.e., for j_ℓ at or below 0.3m s^{-1} and j_g below 0.6m s^{-1}.

4.2.2. Pressure drop vs. gas volumetric flux

In addition to liquid holdup, the experimental results include the overall pressure change along the pipe. Given the measured holdup, the hydrostatic pressure contribution is calculated, and the frictional pressure drop can be determined under the assumption that only friction and gravity contribute to the pressure gradient.

This section presents the calculation results employing the friction models of Table 3. In these calculations, no slip between the phases is assumed.

Fig. 8 shows the downward-flow measured and calculated frictional pressure gradients as a function of gas volumetric flux, j_g, with error bands indicating the estimated experimental uncertainty. The Beggs & Brill model consistently overpredicts the

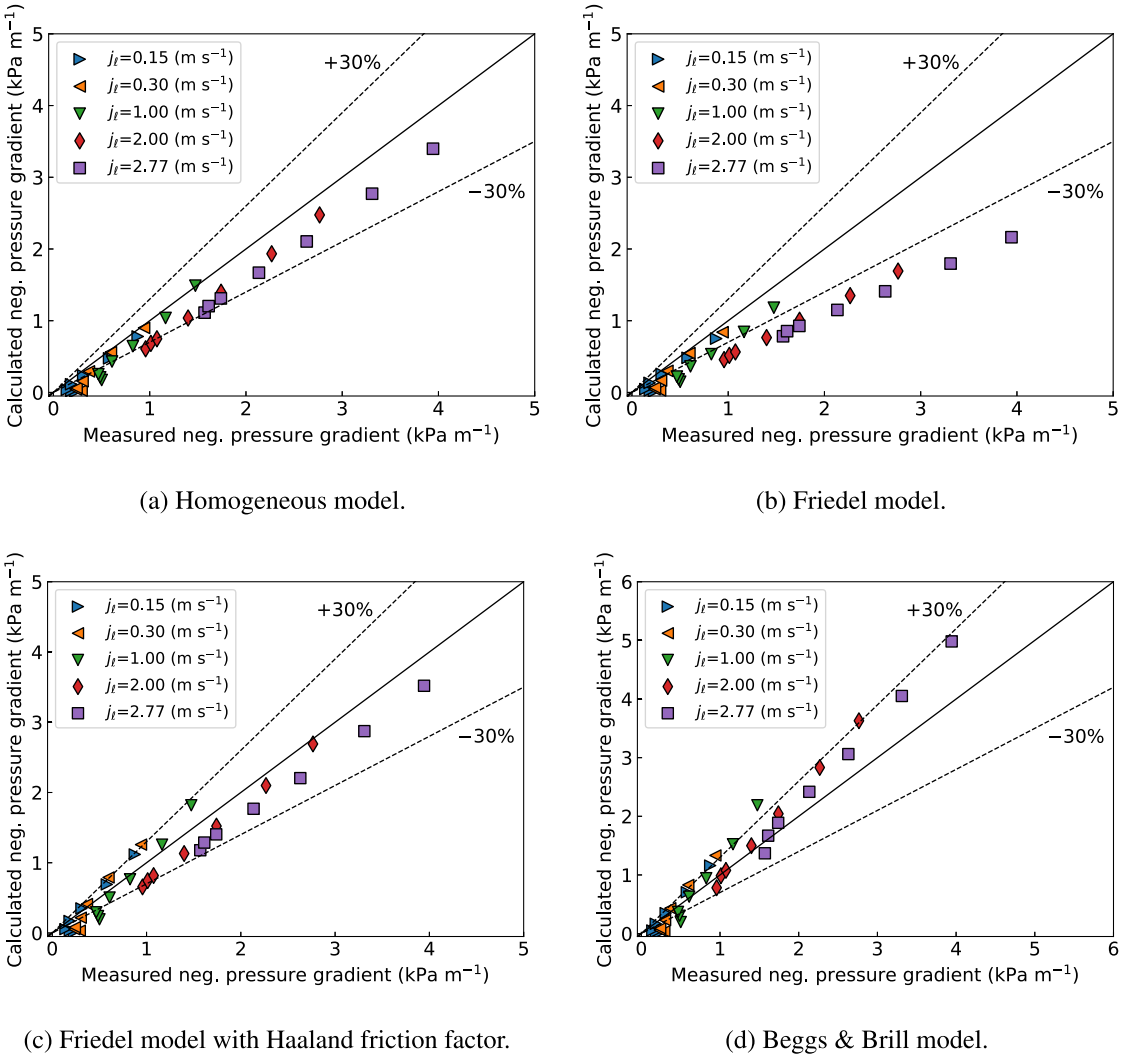

(a) Homogeneous model.

(b) Friedel model.

(c) Friedel model with Haaland friction factor.

(d) Beggs & Brill model.

Fig. 13. Upward flow: Comparison between measured and computed frictional pressure drop for different friction models.

friction. This is also the case for the homogeneous model, but the overprediction is significantly smaller. The Friedel and Friedel (Haaland) models underpredict the friction for liquid volumetric fluxes over 1m s^{-1}, while there is quite good agreement between the Friedel (Haaland) model and experiments for lower liquid volumetric fluxes, and good agreement in general for low gas volumetric fluxes.

We observe that the experimental uncertainty is significant, especially for low fluxes. One reason for this is that the experiment measures the total pressure difference, and the frictional pressure drop is calculated by subtracting the contribution of gravity, which in this case is the dominant part. However, the good agreement between the correlations and the experiments at low gas volumetric fluxes, may indicate that the experimental uncertainty is somewhat overestimated.

Fig. 9 shows the upward-flow measured and calculated (negative) frictional pressure gradient as a function of gas volumetric flux, j_g. There is fair agreement between models and experiments, with some exceptions: In this case, the Friedel model seems to generally underpredict the friction for the higher liquid volumetric fluxes, whereas the Beggs & Brill model overpredicts the friction for the higher gas volumetric fluxes. Further, none of the models are able to predict the friction trends for j_g below 0.6m s^{-1} and j_ℓ at 1.0m s^{-1} and lower, where the measured friction is much higher than the model predictions. Nevertheless, the deviations in this region are smaller than the experimental uncertainty.

4.3. Quantitative model performance

In order to quantify the model performance, we calculate the root-mean-square (RMS) deviation (or 2-norm) between the model prediction, y_{calc}, and the experimental measurement, y_{exp}:

$$\delta_{\text{rms}} = \sqrt{\frac{1}{n}\sum_{i=1}^{n}\left(y_{\text{calc},i} - y_{\text{exp},i}\right)^2}. \tag{13}$$

4.3.1. Liquid holdup

Table 5 gives the root-mean-square deviation between the holdup predictions and the experimental holdup from the X-ray measurements. For upward flow, the no-slip model performs best overall, whereas the no-slip model, the Zuber-Findlay model and the Shi model perform similarly for downward flow. The same can be seen from Figs. 10 and 11, where the performance of the different models are visualized by plotting predicted holdup against measured holdup, for downward and upward flow, respectively. The figures include dashed lines indicating ±30% deviation. Fig. 10(c) shows that the T2Well model underpredicts the holdup

Table 5
RMS deviations between calculations and experiments for liquid holdup (–).

Data	no-slip	T2Well	Zuber	hi
downward, all data	0.025	0.059	0.028	0.027
downward, $j_\ell = 0.15$ m s^{-1}	0.036	0.072	0.035	0.026
downward, $j_\ell = 0.30$ m s^{-1}	0.017	0.082	0.034	0.026
downward, $j_\ell = 1.00$ m s^{-1}	0.021	0.053	0.025	0.030
downward, $j_\ell = 2.00$ m s^{-1}	0.022	0.038	0.021	0.028
downward, $j_\ell = 2.77$ m s^{-1}	0.022	0.033	0.020	0.027
upward, all data	0.015	0.061	0.075	0.036
upward, $j_\ell = 0.15$ m s^{-1}	0.020	0.101	0.098	0.059
upward, $j_\ell = 0.30$ m s^{-1}	0.017	0.086	0.097	0.050
upward, $j_\ell = 1.00$ m s^{-1}	0.011	0.028	0.063	0.011
upward, $j_\ell = 2.00$ m s^{-1}	0.016	0.019	0.053	0.016
upward, $j_\ell = 2.77$ m s^{-1}	0.011	0.016	0.048	0.012

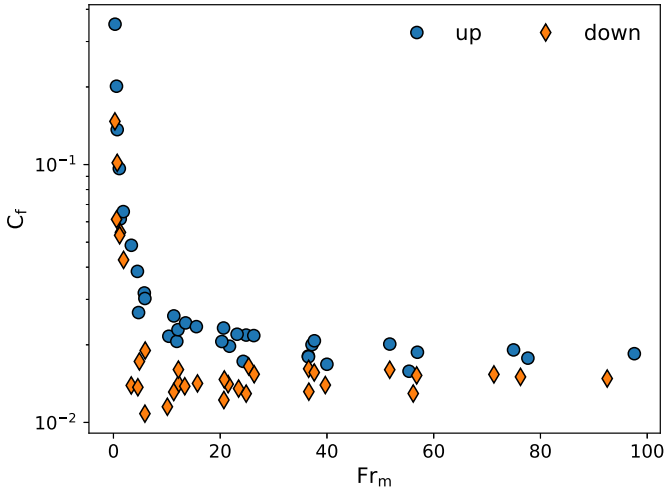

Fig. 14. Dimensionless frictional pressure gradient versus mixture Froude number.

for downward flow, and from Fig. 11(c) we see that the same model overpredicts the holdup for upward flow. We observe from Figs. 10(d) and 11(d) that the Zuber-Findlay model slightly overpredicts the holdup for downward flow, whereas the overprediction is large for upward flow at low volumetric fluxes. The no-slip model, on the other hand, predicts the upward flow rather well (Fig. 11(a)) whereas it underpredicts the holdup for downward flow (Fig. 10(a)). The Shi model performs similarly to the T2Well model for high measured holdups, but for low holdups, it has a lower underprediction for downward flow (Fig. 10(b)) and a lower overprediction for upward flow (Fig. 11(b)).

4.3.2. Frictional pressure drop

Table 6 displays the root-mean-square deviation between the calculated and measured frictional pressure gradient. The Friedel (Haaland) model and the Beggs & Brill model perform better for upward than for downward flow. The homogeneous model is by far the best for the downward flow, while the homogeneous model, Friedel (Haaland) and Beggs & Brill have a similar performance for upward flow.

From the error plots for the downward flow in Fig. 12, we observe that the homogeneous model (Fig. 12(a)) is the only model with the correct behaviour at high volumetric fluxes, where both variants of the Friedel model (Figs. 12(b) and 12(c)) underpredict the friction. The Beggs & Brill model (Fig. 12(d)) consistently overpredicts the pressure drop.

From the error plots for the upward flow in Fig. 13, we see that all models behave reasonably well, except the Friedel model (Fig. 13(b)), which underpredicts the friction due to the lack of a term for the pipe roughness.

4.4. Differences between upward and downward flow

As was observed in Figs. 4–5, the differences in flow regime between upward and downward flow are limited in the present case. A main reason for this is the low values for the gas/liquid property ratios, μ_ℓ/μ_g and ρ_ℓ/ρ_g, both approximately equal to 2.8. Nevertheless, some differences between upward and downward flow can be seen. To illustrate this, in Fig. 14 we have plotted the dimensionless frictional pressure drop as a function of mixture Froude number, for both upward and downward flow. It is a clear trend that the frictional pressure drop is higher for upward flow. We also observe that the data, particularly for upward flow, appear to be well correlated by the Froude number. For downward flow, there is more scatter, which might be related to flow-regime variations, or the increased experimental uncertainty due to the fact that friction and gravity have opposite effects.

A further illustration is given in Fig. 15, where upward and downward flow data, for the highest and lowest liquid volumetric flux. It can be seen that for the liquid holdup (Fig. 15(b)), the differences are small and mostly within the experimental uncertainty. This is consistent with the observation made for Figs. 2–3. However, for the frictional pressure drop (Fig. 15(a)), the values are

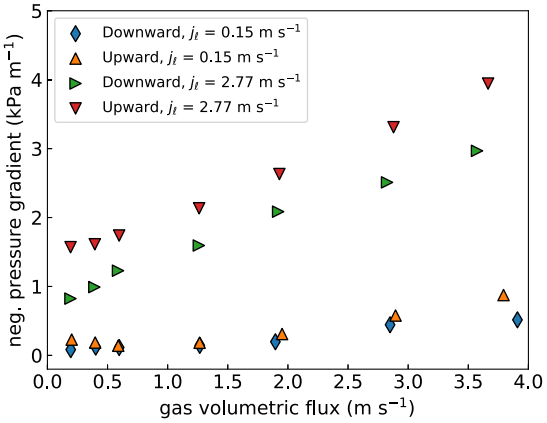

(a) Frictional pressure drop

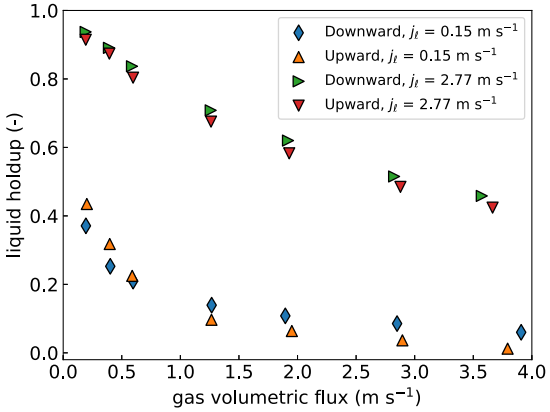

(b) Liquid holdup.

Fig. 15. Measured frictional pressure drop and liquid holdup: Comparison between upward and downward flow.

Table 6
RMS deviations between calculated and measured frictional pressure gradient (kPa m^{-1}).

Data	Homogeneous	Friedel	Friedel (Haaland)	Beggs & Brill
downward, all data	0.123	0.642	0.398	0.644
downward, $j_\ell = 0.15$ m s^{-1}	0.138	0.090	0.129	0.378
downward, $j_\ell = 0.30$ m s^{-1}	0.082	0.157	0.075	0.320
downward, $j_\ell = 1.00$ m s^{-1}	0.138	0.332	0.159	0.533
downward, $j_\ell = 2.00$ m s^{-1}	0.091	0.824	0.527	0.739
downward, $j_\ell = 2.77$ m s^{-1}	0.152	1.113	0.682	1.000
upward, all data	0.293	0.640	0.250	0.357
upward, $j_\ell = 0.15$ m s^{-1}	0.128	0.125	0.146	0.158
upward, $j_\ell = 0.30$ m s^{-1}	0.155	0.156	0.197	0.218
upward, $j_\ell = 1.00$ m s^{-1}	0.210	0.295	0.215	0.335
upward, $j_\ell = 2.00$ m s^{-1}	0.334	0.726	0.233	0.414
upward, $j_\ell = 2.77$ m s^{-1}	0.484	1.181	0.389	0.529

higher for upward flow. This tendency is more significant for the higher liquid volumetric flux. By inspecting Figs. 8–9, we see that the Friedel correlation (both versions) captures this trend, at least for higher gas volumetric flux. The Beggs & Brill correlation captures the increased frictional pressure drop for upward flow only to a smaller extent. The homogeneous model only caters for two-phase flow via the liquid holdup and therefore does not predict any difference between upward and downward flow.

5. Conclusion

Measurements of liquid holdup, pressure drop and flow regime have been made for upward and downward flow of CO_2 in a pipe of inner diameter 44mm at a pressure of 6.5MPa. While this pressure is relatively close to the critical pressure (7.38MPa), giving small differences in the thermophysical properties of gas and liquid, we expect the flow to be genuinely two-phase. This condition is relevant for CO_2-injection wells, which may well be operated such that part of the well contains CO_2 in a two-phase state.

The experimental results indicate that the flow is close to no-slip – within the experimental uncertainty. We have compared the experimental data to well-known models for phase slip and frictional pressure drop. The results show that overall, the best model is the simplest one – the fully homogeneous approach, in which no slip is assumed and the friction is calculated simply by employing gas-liquid mixture properties in the single-phase friction model.

In particular, the homogeneous model performs best for liquid holdup for upward flow and for frictional pressure drop for downward flow. For frictional pressure drop for upward flow, and for liquid holdup for downward flow, several models performed similarly.

The fact that the homogeneous model worked best overall, indicates that the other models tested do not correctly capture the flow behaviour when the gas and liquid phase properties become similar close to the critical point.

Declaration of Competing Interest

The authors declare that they have no known competing financial interests or personal relationships that could have appeared to influence the work reported in this paper.

CRediT authorship contribution statement

Morten Hammer: Methodology, Software, Investigation, Data curation, Writing - original draft, Writing - review & editing, Visualization. **Han Deng:** Software, Formal analysis, Investigation, Data curation, Writing - review & editing, Visualization. **Lan Liu:** Investigation, Data curation, Writing - review & editing. **Morten Langsholt:** Methodology, Investigation, Resources, Writing - review & editing. **Svend Tollak Munkejord:** Conceptualization, Writing - original draft, Writing - review & editing, Supervision, Funding acquisition.

Acknowledgements

ACT ELEGANCY, Project No 271498, has received funding from DETEC (CH), BMWi (DE), RVO (NL), Gassnova (NO), BEIS (UK), Gassco, Equinor and Total, and is cofunded by the European Commission under the Horizon 2020 programme, ACT Grant Agreement No 691712.

Appendix A. Experimental data

The experimental data tables for upward and downward flow are attached as supplementary files.

Supplementary material

Supplementary material associated with this article can be found, in the online version, at doi: 10.1016/j.ijmultiphaseflow.2021.103590.

References

Aursand, P., Hammer, M., Lavrov, A., Lund, H., Munkejord, S.T., Torsæter, M., 2017. Well integrity for CO_2 injection from ships: Simulation of the effect of flow and material parameters on thermal stresses. Int. J. Greenh. Gas Con. 62, 130–141. doi:10.1016/j.ijggc.2017.04.007. Jul.

Ayachi, F., Tauveron, N., Tartiére, T., Colasson, S., Nguyen, D., 2016. Thermo-electric energy storage involving CO_2transcritical cycles and ground heat storage. Appl. Therm. Eng. 108, 1418–1428. doi:10.1016/j.applthermaleng.2016.07.063. Sep.

Ayub, A., Invernizzi, C.M., Di Marcoberardino, G., Iora, P., Manzolini, G., 2020. Carbon dioxide mixtures as working fluid for high-temperature heat recovery: a thermodynamic comparison with transcritical organic rankine cycles. Energies 13 (15), 4014. doi:10.3390/en13154014.

Balay, S., Abhyankar, S., Adams, M. F., Brown, J., Brune, P., Buschelman, K., Dalcin, L., Dener, A., Eijkhout, V., Gropp, W. D., Kaushik, D., Knepley, M. G., May, D. A., McInnes, L. C., Mills, R. T., Munson, T., Rupp, K., Sanan, P., Smith, B. F., Zampini, S., Zhang, H., Zhang, H., 2018. PETSc Web page. http://www.mcs.anl.gov/petsc.

Balay, S., Gropp, W.D., McInnes, L.C., Smith, B.F., 1997. Efficient management of parallelism in object oriented numerical software Libraries. In: Arge, E., Bruaset, A.M., Langtangen, H.P. (Eds.), Modern Software Tools in Scientific Computing. Birkhäuser Press, pp. 163–202.

Beggs, H.D., Brill, J.P., 1973. A study of two-phase flow in inclined pipes. In: J. Petrol. Technol., pp. 607–617. Doi:10.2118/4007-PA

Collier, J.G., Thome, J.R., 1994. Convective Boiling and Condensation, third Oxford University Press, Oxford, UK. ISBN 0-19-856282-9

Cronshaw, M.B., Bolling, J.D., 1982. A numerical model of the non-isothermal flow of carbon dioxide in wellbores. SPE California Regional Meeting. Society of Petroleum Engineers, San Francisco, California, USA. Doi:10.2118/10735-MS. Paper SPE-10735-MS.

Dorao, C.A., Ryu, J., Fernandino, M., 2019. Law of resistance in two-phase flows inside pipes. Appl. Phys. Lett. 114 (17), 173704. doi:10.1063/1.5082808.

Drew, D.A., Passman, S.L., 1999. Theory of Multicomponent Fluids, vol. 135 of Applied Mathematical Sciences. Springer-Verlag, New York. ISBN 0-387-98380-5

Edenhofer, O., Pichs-Madruga, R., Sokona, Y., Farahani, E., Kadner, S., Seyboth, K., Adler, A., Baum, I., Brunner, S., Eickemeier, P., Kriemann, B., Savolainen, J.,

Schlømer, S., von Stechow, C., Zwickel, T., M., J., 2014. Climate change 2014: mitigation of climate change. Tech. rep., Working Group III Contribution to the Fifth Assessment Report of the Intergovernmental Panel on Climate Change, Summary for Policymakers, IPCC.. http://mitigation2014.org/.

Eter, A., Groeneveld, D., Tavoularis, S., 2017. Convective heat transfer in supercritical flows of CO_2 in tubes with and without flow obstacles. Nucl. Eng. Design 313, 162–176. doi:10.1016/j.nucengdes.2016.12.016.

Farokhpoor, R., Liu, L., Langsholt, M., Hald, K., Amundsen, J., Lawrence, C., 2020. Dimensional analysis and scaling in two-phase gas-liquid stratified pipe flow – methodology evaluation. Int. J. Multiphase Flow 122, 103139. doi:10.1016/j.ijmultiphaseflow.2019.103139.

Fenghour, A., Wakeman, W.A., Vesovic., V., 1998. The viscosity of carbon dioxide. J. Phys. Chem. Ref. Data 27 (1), 31–44. doi:10.1063/1.556013.

Friedel, L., 1979. Improved friction pressure drop correlations for horizontal and vertical two phase pipe flow. In: Proceedings, European Two Phase Flow Group Meeting. Ispra, Italy. Paper E2

Gjennestad, M.A., Gruber, A., Lervåg, K.Y., Johansen, O., Ervik, Å., Hammer, M., Munkejord, S.T., 2017. Computation of three-dimensional three-phase flow of carbon dioxide using a high-order WENO scheme. J. Comput. Phys. 348, 1–22. doi:10.1016/j.jcp.2017.07.016.

Haaland, S.E., 1983. Simple and explicit formulas for the friction factor in turbulent pipe flow. J. Fluid Eng. – T. ASME 105 (1), 89–90. doi:10.1115/1.3240948.

Håvelsrud, M., 2012. Improved and verified models for flow of CO_2 in pipelines. In: The Third International Forum on the Transportation of CO_2 by Pipeline. Clarion Technical Conferences, Gateshead, UK..

Hammer, M., Aasen, A., Wilhelmsen, Ø., 2020. Thermopack. https://github.com/SINTEF/thermopack/. Accessed 2020-12-15.

Hewitt, G. F., 2011. Pressure Drop, Two-phase Flow. www.thermopedia.com. Doi:10.1615/AtoZ.p.pressure_drop_two-phase_flow. Accessed 2020-08-27.

Hibiki, T., Ishii, M., 2002. Development of one-group interfacial area transport equation in bubbly flow systems. Int. J. Heat Mass Tran. 45 (11), 2351–2372. doi:10.1016/S0017-9310(01)00327-1.

IEA, 2017. Energy Technology Perspectives. ISBN 978-92-64-27597-3 Doi:10.1787/energy_tech-2017-en.

Ishii, M., 1977. Drift flux model and derivation of kinematic consitutive laws. In: Kakaç, S., Mayinger, F. (Eds.), Proceedings of NATO Advanced Study Institute. Aug. Hemisphere, pp. 187–208.

Joint Committee for Guides in Metrology, 2008. Evaluation of Measurement Data – Guide to the Expression of Uncertainty in Measurement. JCGM 100, 2008. https://www.bipm.org/utils/common/documents/jcgm/JCGM_100_2008_E.pdf.

Knoll, D.A., Keyes, D.E., 2004. Jacobian-free Newton–Krylov methods: a survey of approaches and applications. J. Comput. Phys. 193 (2), 357–397. doi:10.1016/j.jcp.2003.08.010.

Li, X., Li, G., Wang, H., Tian, S., Song, X., Lu, P., Wang, M., 2017. A unified model for wellbore flow and heat transfer in pure CO_2injection for geological sequestration, EOR and fracturing operations. Int. J. Greenh. Gas Con. 57, 102–115. doi:10.1016/j.ijggc.2016.11.030.

Lorentzen, G., 1994. Revival of carbon dioxide as a refrigerant. Int. J. Refrig. 17 (5), 292–301. doi:10.1016/0140-7007(94)90059-0.

Lu, M., Connell, L.D., 2014. Transient, thermal wellbore flow of multispecies carbon dioxide mixtures with phase transition during geological storage. Int. J. Multiphase Flow 63, 82–92. doi:10.1016/j.ijmultiphaseflow.2014.04.002.

Moe, A.M., Dugstad, A., Benrath, D., Jukes, E., Anderson, E., Catalanotti, E., Durusut, E., Neele, F., Grunert, F., Mahgerefteh, H., Gazendam, J., Barnett, J., Hammer, M., Span, R., Brown, S., Munkejord, S.T., Weber, V., 2020. A trans-European delcoto transportation infrastructure for CCUS: Opportunities & challenges. Report, Zero Emissions Platform, Brussels, Belgium.. Available from https://zeroemissionsplatform.eu/wp-content/uploads/A-Trans-European-CO2-Transportation-Infrastructure-for-CCUS-Opportunities-Challenges.pdf.

Munkejord, S.T., Bernstone, C., Clausen, S., de Koeijer, G., Mølnvik, M.J., 2013. Combining thermodynamic and fluid flow modelling for CO_2flow assurance. In: Dixon, T., Yamaji, K. (Eds.), GHGT-11 – 11th International Conference on Greenhouse Gas Control Technologies. RITE / IEAGHGT, Energy Procedia, Kyoto, Japan, pp. 2904–2913. Vol. 37 Doi:10.1016/j.egypro.2013.06.176

Munkejord, S.T., Hammer, M., Ervik, Å., Odsæter, L.H., Lund, H., 2020. Coupled CO_2-well-reservoir simulation using a partitioned approach: effect of reservoir properties on well dynamics. Greenh. Gas. Sci. Tech.. doi: 10.1002/ghg.2035.

Munkejord, S.T., Hammer, M., Løvseth, S.W., 2016. CO_2transport: Data and models – A review. Appl. Energ. 169, 499–523. doi:10.1016/j.apenergy.2016.01.100.

Osher, S., Fedkiw, R.P., 2001. Level set methods: An overview and some recent results. J. Comput. Phys. 169 (2), 463–502. doi:10.1006/jcph.2000.6636.

Pan, L., Oldenburg, C.M., Pruess, K., Wu, Y.S., 2011. Transient CO_2 leakage and injection in wellbore-reservoir systems for geologic carbon sequestration. Greenh. Gas. Sci. Tech. 1 (4), 335–350. doi:10.1002/ghg.41.

Pan, L., Oldenburg, C.M., Wu, Y.-S., Pruess, K., 2011. T2Well/ECO2N version 1.0 manual: multiphase and non-isothermal model for coupled wellbore-reservoir flow of carbon dioxide and variable salinity water. Tech. Rep. LBNL-4291E, Earth Sciences Division, Lawrence Berkeley National Laboratory.

Pettersen, J., Rieberer, R., Munkejord, S.T., 2000. Heat transfer and pressure drop characteristics of evaporating carbon dioxide in microchannel tubes. In: 4th IIR Gustav Lorentzen Conference on Natural Working Fluids. IIF-IIR Commission B1, B2, E1, and E2, Purdue University, USA.

Rathjen, W., Straub, J., 1977. Temperature dependence of surface tension, coexisting curve, and vapor pressure of CO_2, $CClF_3$, $CBrF_3$, and SF_6. In: Hahne, E., Grigull, U. (Eds.), Heat Transfer in Boiling. Taylor & Francis Inc.. Chap. 18. ISBN 0-123-14450-7

Sacconi, A., Mahgerefteh, H., 2020. Modelling start-up injection of CO_2 into highly-depleted gas fields. Energy 191, 116530. doi:10.1016/j.energy.2019.116530.

Sethian, J.A., 2001. Evolution, implementation, and application of level set and fast marching methods for advancing. J. Comput. Phys. 169 (2), 503–555. doi:10.1006/jcph.2000.6657.

Shi, H., Holmes, J.A., Diaz, L.R., Durlofsky, L.J., Aziz, K., 2005. Drift-flux modeling of two-phase flow in wellbores. SPE J. 10 (2), 130–137. doi:10.2118/89836-PA.

Shi, H., Holmes, J.A., Durlofsky, L.J., Aziz, K., Diaz, L.R., Alkaya, B., Oddie, G., 2005. Drift-flux modeling of two-phase flow in wellbores. SPE J. 10 (1), 24–33. doi:10.2118/84228-PA. Mar.

Span, R., Eckermann, T., Herrig, S., Hielscher, S., Jäger, A., Thol, M., 2016. TREND. Thermodynamic reference and engineering data 3.0.. Lehrstuhl für Thermodynamik, Ruhr-Universität Bochum.

Span, R., Wagner, W., 1996. A new equation of state for carbon dioxide covering the fluid region from the triple-point temperature to 1100 K at pressures up to 800 MPa. J. Phys. Chem. Ref. Data 25 (6), 1509–1596. doi:10.1063/1.555991.

Stewart, H.B., Wendroff, B., 1984. Two-phase flow: Models and methods. J. Comput. Phys. 56 (3), 363–409. doi:10.1016/0021-9991(84)90103-7.

RELAP5 Development Team, 1995. RELAP5/MOD3 code manual: Models and correlations. Code Manual NUREG/CR-5535. INEL-95/0174, vol. 4, U.S. Nuclear Regulatory Commission, Washington DC, USA. Available from https://www.nrc.gov/docs/ML1103/ML110330271.pdf.

Tryggvason, G., Bunner, B., Esmaeli, A., Juric, D., Al-Rawahi, N., Tauber, W., Han, J., Nas, S., Jan, Y.J., 2001. A front-tracking method for the computations of multiphase flow. J. Comput. Phys. 169 (2), 708–759. doi:10.1006/jcph.2001.6726.

Vesovic, V., Wakeham, W.A., Olchowy, G.A., Sengers, J.V., Watson, J.T.R., Millat, J., 1990. The transport properties of carbon dioxide. J. Phys. Chem. Ref. Data 19, 763–808. doi:10.1063/1.555875.

White, F.M., 1994. Fluid Mechanics, third McGraw-Hill, Inc., New York. ISBN 0-07-911695-7.

Wilhelmsen, Ø., Aasen, A., Skaugen, G., Aursand, P., Austegard, A., Aursand, E., Gjennestad, M.A., Lund, H., Linga, G., Hammer, M., 2017. Thermodynamic modeling with equations of state: present challenges with established methods. Ind. Eng. Chem. Res. 56 (13), 3503–3515. doi:10.1021/acs.iecr.7b00317.

Zou, L., Zhao, H., Zhang, H., 2016. Application of Jacobian-free Newton–Krylov method in implicitly solving two-fluid six-equation two-phase flow problems: implementation, validation and benchmark. Nucl. Eng. Design 300, 268–281. doi:10.1016/j.nucengdes.2016.01.033.

Zuber, N., Findlay, J.A., 1965. Average volumetric concentration in two-phase flow systems. J. Heat Trans. – T. ASME 87, 453–468. doi:10.1115/1.3689137.